Mon. Not. R. Astron. Soc. **306,** 427–436 (1999)

Partition function based analysis of cosmic microwave background maps

J. M. Diego,[1,2] E. Martínez-González,[1] J. L. Sanz,[1] Silvia Mollerach[3,4] and Vicent J. Martínez[3]

[1]*Instituto de Física de Cantabria, Consejo Superior de Investigaciones Científicas Universidad de Cantabria, Santander, Spain*
[2]*Departamento de Física Moderna, Universidad de Cantabria, Avda. Los Castros s/n, 39005 Santander, Spain*
[3]*Departamento de Astronomía y Astrofísica, Universitat de València, 46100 Burjassot, Valencia, Spain*
[4]*Departamento de Física, Universidad Nacional de La Plata, c.c. 67, 1900 La Plata, Argentina*

Accepted 1999 February 4. Received 1999 February 3; in original form 1998 October 23

ABSTRACT

We present an alternative method to analyse cosmic microwave background (CMB) maps. We base our analysis on the study of the partition function. This function is used to examine the CMB maps, making use of the different information embedded at different scales and moments.

Using the partition function in a likelihood analysis in two dimensions ($Q_{\rm rms-PS}$,n), we find the best-fitting model to the best data available at present (the *COBE*–DMR 4 years data set). By means of this analysis we find a maximum in the likelihood function for $n = 1.8^{+0.35}_{-0.65}$ and $Q_{\rm rms-PS} = 10^{+3}_{-2.5}$ μK (95 per cent confidence level) in agreement with the results of other similar analyses [Smoot et al. (1 yr), Bennet et al. (4 yr)].

Also making use of the partition function we perform a multifractal analysis and study the possible fractal nature of the CMB sky. We find that the measure used in the analysis is not a fractal. Finally, we use the partition function for testing the statistical distribution of the *COBE*–DMR data set. We conclude that no evidence of non-Gaussianity can be found by means of this method.

Key words: methods: data analysis – cosmic microwave background.

1 INTRODUCTION

In a few years the forthcoming CMB data sets from the *MAP* (NASA) and *PLANCK* (ESA) missions will offer us a much better image of the young Universe than ever before. The CMB represents a view of the Universe when it was about 0.002 per cent of its present age. CMB anisotropies provide a link between theoretical predictions and observational data. Undoubtedly these data will constrain more accurately the fundamental cosmological parameters. In recent years several groups have been very active in the study of the CMB anisotropies. Many statistical methods have been adapted to the analysis of the future CMB maps, and others are being developed.

There are many methods that can give relatively accurate values for the parameters of the cosmological models. For example, the power spectrum is considered to be the best discriminator between different models (Bond, Efstathiou & Tegmark 1997; Hinshaw et al. 1996a; Wright et al. 1996; Tegmark 1996). Related through a Legendre expansion to the power spectrum, the two-point correlation function is also a useful discriminator (Cayón et al 1996; Hinshaw et al 1996b). These analyses, based on the power spectrum, are considered as *classical* but there are many other methods that do not make use of the power spectrum. The quality of the CMB maps demands for other statistics to supplement the power spectrum, looking for instance at morphological or topological characteristics of the data. For example, the one-dimensional analysis is a geometrical method useful for one-dimensional scans of CMB data and is based on the study of regions above or below a certain level (Gutiérrez et al. 1994). The peak analyses, similar to the previous one but for two-dimensional data, deal with the number of spots above a given threshold (Fabbri & Torres 1995) or with other geometrical properties like the Gaussian curvature or excentritity of the maxima (Barreiro et al. 1997). Other approaches are the genus (Smoot et al. 1994; Torres et al. 1995), Minkowski functionals, which relate several geometrical aspects at the same time (Schmalzing & Górski 1997; Winitzki & Kosowsky 1997), wavelet-based techniques (Pando, Valls-Gabaud & Fang 1998; Hobson, Jones & Lasenby 1998) who have shown wavelets to be very effective at detecting non-Gaussianity in the CMB, and fractality (Pompilio et al. 1995; De Gouveia dal Pino et al. 1995; Mollerach et al. 1998).

In this paper we present an alternative method to analyse CMB maps based on the partition function. This function contains useful information about the temperature anisotropies at the different scales and moments. The method presented here is related to the one used by Smoot et al. (1994) based on moments at different smoothing angles. However, our method is more general and powerful because it works with any moment, not only with positive and integer ones.

The structure of the paper is as follows. In Section 2 we present the partition function and discuss its main characteristics. In the same section three different analyses based on that function are introduced: a likelihood analysis, a multifractal analysis and a test of Gaussianity. The likelihood analysis uses the partition function to search for the parameters ($Q_{\rm rms-PS}$ and n) that best fit a given data set. The multifractal analysis searches for scaling laws and fractal behaviour of the data. There are theoretical reasons (Sachs–Wolfe effect) to expect scaling in the data. Here we present the generalized fractal dimensions and the scaling exponents and also comment on the possible multifractality of the CMB sky. In a recent paper, Ferreira, Magueijo & Górski (1998) found evidence of non-Gaussianity in *COBE*–DMR data at the 99 per cent confidence level. We show that the partition function can be used to study this property. There is a clear relation between the partition function and the cumulant function, the last one having a specific form for a Gaussian signal. In Section 3 we apply the results of the previous sections to the *COBE*–DMR 4 years data set and we compare this with other results. We conclude in Section 4.

2 THE PARTITION FUNCTION

Let us start directly with the definition,

$$Z(q,\delta) = \sum_{i=1}^{N_{\rm boxes}(\delta)} \mu_i(\delta)^q \tag{1}$$

where $Z(q,\delta)$ is the partition function. The quantity $\mu_i(\delta)$ is called the *measure*, it is a function of δ which is the size or scale of the boxes used to cover the sample. The boxes are labelled by i, and $N_{\rm boxes}(\delta)$ is the number of boxes (or cells) needed to cover the map when the grid with resolution δ is used. The exponent q is a continuous real parameter that plays the role of the order of the moment of the measure.

Let us consider a map of N pixels. Now the map is divided in boxes of size $\delta \times \delta$ pixels and the measure $\mu_i(\delta)$ is computed in each one of the resulting boxes. Changing both, q and δ, one calculates the function $Z(q,\delta)$. We would like to emphasize that the calculation of $Z(q,\delta)$ is $O(N)$.

One is free to make any choice of the measure $\mu(\delta)$ provided that several conditions are satisfied, the most restrictive being $\mu_i(\delta) \geq 0$. There are no general rules to decide which is the best choice. For CMB maps, we use the most natural measure defined as follows:

$$\mu_i(\delta) = \frac{1}{T_*} \sum_{{\rm pix}_j \in {\rm box}_i} T_{{\rm pix}_j}. \tag{2}$$

Thus the measure in the box i is the sum of the *absolute* temperatures $T_{\rm pix}$ of the pixels inside the box in units of Kelvin. This is a very natural measure comparable to the measure used in the study of galaxies or clusters distribution (Martínez et al. 1990, see Borgani 1995 for a review), where the measure is taken as the total mass (or the total number of galaxies/clusters) contained in the box. The constant T_* is a normalization constant. The measures are interpreted as probabilities and they have to be normalized, i.e $\sum_i \mu_i = 1$. So T_* is simply the sum of the absolute temperatures over all pixels and therefore is a constant for all boxes and scales.

The temperature in the pixels is almost the same everywhere because of the homogeneity of the signal, and one expects that different models will behave in a very similar way, making difficult the task of distinguishing them. We shall show how the partition function overcomes this problem.

Alternatively, Pompilio et al. (1995), in a multifractal analysis of string-induced CMB anisotropies (one-dimensional scans) used as a measure

$$\mu_i(\delta) = \sum_{j=i-M\delta/2}^{j=i+M\delta/2} [\Delta_j - \Delta_{j+1}]^2, \tag{3}$$

where Δ_j denotes the fluctuation of the temperature in pixel j with respect to the mean. Here M is the total number of points in the data set, and $(i - M\delta/2)$ and $(i + M\delta/2)$ are the lower and upper edges of the ith segment with $M \times \delta$ points, centred on the ith point of the scan. The scale δ runs between $1/M$ for the smallest segment and 1 for the whole segment. However, this measure is not sensitive to the sign of the temperature fluctuations because of the square in its definition. As a result of this fact the full information of the fluctuations is not conveniently considered. In addition, the generalization of this measure to 2D maps is not unique. Using the measure proposed in this paper, the differences between two-temperature data sets appear when high values of the exponent q are considered. The method is able to differentiate between two very close models with a q range of $[-2.5\times10^5, +2.5\times10^5]$. This range for q is in agreement with the level of inhomogeneity. We are using *absolute* temperatures, that is, we have inhomogeneities of order 10^{-5} with respect to the mean value and the signal is almost flat. One can consider q as a powerful microscope, able to enhance the smallest differences of two very similar maps. Furthermore, q is a selective parameter. Choosing large values of q in the partition function, favours contributions from cells with relatively high values of $\mu_i(\delta)$ since $\mu_i^q \gg \mu_j^q$ for $\mu_i > \mu_j$, if $q \gg 0$. Conversely, $q \ll 0$ favours the cells with relatively low values of the measure. This is the role played by the moments, changing q one explores the different parts of the measure probability distribution. The other parameter, δ, acts like a filter. Choosing large values of δ is similar to apply a large-scale filter to the map. One looks at different scales when the parameter δ is changed.

To summarize, $Z(q,\delta)$ contains information at different scales and moments. The multi-scale information gives an idea of the correlations in the map, meanwhile the moments are sensitive to possible asymmetries in the data, as well as some deviations from Gaussianity. In what follows we show the power of the partition function to extract useful information from CMB data. Three different analyses are used for this purpose.

2.1 Likelihood analysis

We shall use the partition function to encode the information of a given map. We compute it both for the experimental data and for simulated ones corresponding to different models. In this process we are comparing the data and the models at several scales and using different moments. If there are some differences at some scale or moment, then the partition function should make it evident. The likelihood function will have a maximum for the best-fitting model to the data. For the CMB maps analyses, we consider models corresponding to different values of the spectral index n and the normalization $Q_{\rm rms-PS}$.

The likelihood is defined in the usual way [assuming a Gaussian distribution for $\ln Z(q,\delta)$]. We work with $\mathcal{Z} = \ln Z(q,\delta)$ instead of $Z(q,\delta)$ because of the large values of q, which make imposible to compute directly $Z(q,\delta)$,

$$L(Q_{\rm rms-PS}, n) = \frac{1}{(2\pi)^{n/2}({\rm det}M)^{1/2}} \exp\left(-\frac{1}{2}\chi^2\right), \tag{4}$$

where,

$$\chi^2 = \sum_{i=1}^{N_p}\sum_{j=1}^{N_p}[\langle\mathcal{Z}(i)\rangle - \mathcal{Z}_D(i)]M_{ij}^{-1}[\langle\mathcal{Z}(j)\rangle - \mathcal{Z}_D(j)], \quad (5)$$

and $\langle\mathcal{Z}(i)\rangle$ is the average of the $\mathcal{Z}$ for the N_{ea} realizations of the model at bin i. The index i defines pairs of values (q,δ) and runs from 1 to $N_q \times N_\delta$. That is, i runs from 1 to the total number of points N_p where $Z(q,\delta)$ is defined.

$\mathcal{Z}_D(i)$ is the value of $\mathcal{Z}$ for the experimental data at bin i. M_{ij} is the covariance matrix calculated with Monte Carlo realizations:

$$M_{ij} = \frac{1}{N_{ea}}\sum_{k=1}^{N_{ea}}[\mathcal{Z}_k(i) - \langle\mathcal{Z}(i)\rangle][\mathcal{Z}_k(j) - \langle\mathcal{Z}(j)\rangle]. \quad (6)$$

$\mathcal{Z}_k(i)$ denotes the value of $\mathcal{Z}$ at bin i for the k realization.

We tried different number of realizations N_{ea} but the results appear to be stable for $N_{ea} > 2000$ per value of $Q_{\rm rms-PS}$ and n.

We have two possibilities to perform a best fit to the data. The first one is to minimize χ^2 and take the values of $Q_{\rm rms-PS}$ and n at the minimum of the χ^2 surface as the best-fitting values. The second possibility is to work with the likelihood L looking for the maximum. We tested the two possibilities using simulated CMB maps derived from a given pair of parameters $(Q_{\rm rms-PS}, n)$ and then using these maps as the data maps. Owing to cosmic variance we obtain a set of maxima in the likelihood and of minima in the χ^2. The conclusion is that the likelihood is somewhat better than the χ^2 as expected. For instance with 2000 input realizations with $Q_{\rm rms-PS} = 14\,\mu$K and $n = 1.3$ the distribution of maximun likelihood values finds a maximum at $Q_{\rm rms-PS} = 13^{+3}_{-4.25}\,\mu$K and $n = 1.2^{+0.8}_{-0.15}$ while the χ^2 renders a minimum in $Q_{\rm rms-PS} = 17^{+5}_{-4}\,\mu$K and $n = 1.0^{+0.45}_{-0.35}$. The errors are marginalized at the 68 per cent confidence level and are similar to those obtained with the standard methods based on the power spectrum (see for instance Wright et al. 1996).

2.2 Multifractal analysis

The notion of multifractal measure was first introduced by Mandelbrot (Mandelbrot 1974) in order to study different aspects of the intermittency of turbulence (see also Sreenivasan & Menevau 1988). The multifractal formalism was further developed by many other authors and today it is a standard tool applied in almost all fields of science: molecular physics, biology, geology, astronomy, etc . In the context of the description of the large-scale structure of the Universe it was first introduced by Jones et al. (1988).

Some authors (Pietronero, Montuori & Sylos-Labini 1997) suggest that the distribution of matter in the Universe is fractal with dimensionality $D_2 \simeq 2$. They defend that the scaling remains up to the larger scales probed by the currently available redshift catalogues. Many other authors, however, have found enough evidence of homogeneity at large scales (Davis 1997; Guzzo 1997; Scaramella et al. 1998) in the analysis of the same data sets. One of the basic tenets of the standard cosmology is that at very large scales the distribution of matter is homogeneous. The homogeneity and isotropy of the CMB support this overwhelming evidence, indicating that there exists a continuous transition between scale invariant clustering at small scales and homogeneity at large scales (Martínez et al. 1998; Wu, Lahav & Rees 1998).

At large angular scales, the CMB anisotropies $\Delta T/T$ generated from a scale-free density perturbation power spectrum in a flat $\Omega = 1$ universe can be described by a fractional Brownian fractal (as shown in Mollerach et al. 1998). In particular, both inflationary and defect models predict an approximately scale invariant Harrison–Zel'dovich spectrum on large angular scales showing the scaling predicted by the Sachs–Wolfe effect. At small angular scales ($0.2^\circ \leq \theta \leq 1^\circ$) the predictions of inflation and topological defects models are different (Durrer et al. 1997) allowing to differentiate them. It is then interesting to study the possible fractality of the CMB anisotropies, since the seeds or fluctuations that are supposed to be the precursors of the largest structures observed today, are yet unperturbed by evolutionary phenomena. Several works follow this kind of analysis. In the paper by De Gouveia dal Pino et al. (1995), the authors based their analysis in the study of the perimeter-area relation of the isocontours of temperature at a given threshold. They used the *COBE*–DMR 1 year data set and only the 53-GHz channel. They found evidence for a fractal structure in the *COBE*–DMR data with dimension $D = 1.43$ suggesting that the CMB could not be homogeneous. Apart from the fact that these data have a low signal-to-noise ratio, this does not necessarily mean that the CMB is not homogeneous. This dimension corresponds to the temperature isocontours, and not to the temperature itself. Other works use multifractal analysis with CMB. Pompilio et al. (1995) apply the multifractal analysis to simulated string-induced CMB scans searching for the non-Gaussian behaviour induced by cosmic strings. More recently, Mollerach et al. (1998) have applied a fractal analysis in order to study the roughness of the last scattering surface and used this technique to search for the model that best fits the *COBE*–DMR 4yr data. These authors show the capabilities of this method for the analysis of future data, in particular for those experiments with high signal-to-noise ratio. In this section we will use the partition function to study the possible multifractality of the CMB sky, using as measure the absolute temperature (see equation 2). The multifractal analysis has been presented in several versions but the most popular is from Frisch & Parisi (1985), Jensen et al. (1985) and Halsey et al. (1996), where the spectrum of singularities $f(\alpha)$ was introduced. We will give here a brief description of the multifractal approach. A presentation of the method can be found in Feder (1988), Schuster (1989), Vicsek (1989) and more formally in Falconer (1990).

The multifractal formalism has as its starting point the partition function. The generalized or Renyi dimensions are defined by the asymptotic behaviour (as the scale δ tends to zero) of the ratio between $\ln Z(q,\delta)$ and $\ln\delta$,

$$D(q) = \lim_{\delta\to 0}\frac{1}{q-1}\frac{\ln Z(q,\delta)}{\ln\delta}. \quad (7)$$

It is easy to see that for $q = 0$ we obtain the box-counting or capacity dimension,

$$D(0) = \lim_{\delta\to 0}\frac{\ln N_{\rm boxes}(\delta)}{\ln(1/\delta)}. \quad (8)$$

For $q = 1$, $D(1)$ is the information dimension, which is obtained from equation (7) by applying L'Hôpital's rule. For $q = 2$, $D(2)$ is the correlation dimension (see Schuster 1989 for other alternative definitions and the relation between them). A *simple* fractal or *monofractal* is defined by a constant $D(q)$. Dependence of D on q defines a multifractal. In most of the practical applications of the multifractal analysis, the limit in equation (7) cannot be calculated, either because we do not have information for small distances (as it happens in this case) or because below a minimum physical length no scaling can exist at all (for example the size of a galaxy in the multifractal nature of the galaxy distribution). This problem is usually overcome by finding a scaling range $[\delta_1, \delta_2]$ where a

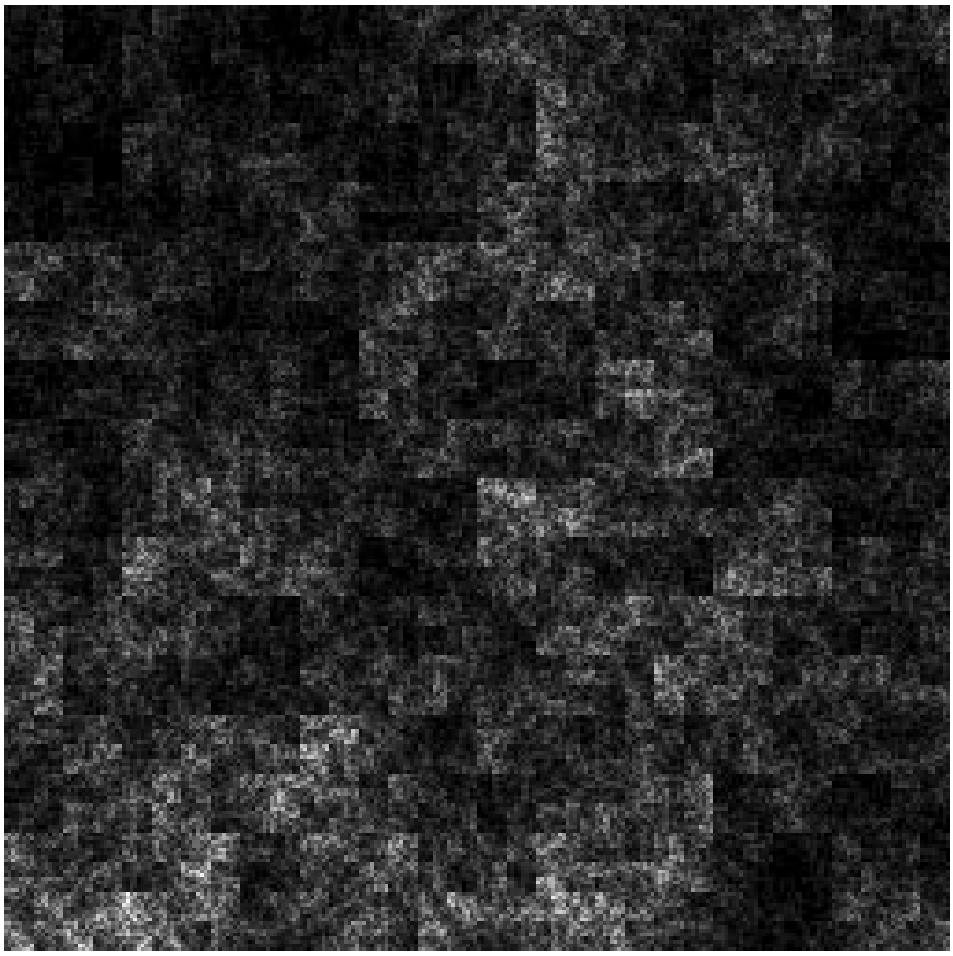

Figure 1. A realization of the multiplicative multifractal on a grid of 25615:43256 pixels. The grey scale denote the strength of the multifractal measure.

power-law can be fitted to the behaviour of the partition function

$$Z(q,\delta) \propto \delta^{\tau(q)} \qquad \text{for} \quad \delta_1 \leq \delta \leq \delta_2. \tag{9}$$

The scaling exponents $\tau(q)$ are related with the generalized dimensions by

$$\tau(q) = (q-1)D(q). \tag{10}$$

Other quantity, commonly used in the characterization of multifractals, is the so-called $f(\alpha)$ spectrum. If for a given box (labelled by j) the measure scales as

$$\mu_j(\delta) \sim \delta^{\alpha_j}, \tag{11}$$

then, the exponent α, which depends in principle on the position is known as crowding index or Hölder exponent. If all the points have the same scaling, then all the exponents α will be the same and this corresponds to a monofractal. Otherwise, if we have boxes with different scaling, what we have is a mixture of monofractals. This set is known as a *multifractal* (each monofractal formed by the points with the same scaling and therefore with the same exponent α). The exponent α is used to label the boxes covering the set supporting a measure, thereby allowing a separate counting for each value of α. In a multifractal set α can take different values within a certain range, corresponding to the different strength of the measure (Halsey et al. 1996). The subset formed by the boxes with the same α will be denoted S_α. This subset has $N_\alpha(\delta)$ elements (boxes) and in general, for a multifractal set, this number varies with the scale δ as

$$N_\alpha(\delta) \sim \delta^{-f(\alpha)}. \tag{12}$$

Comparing this expression with the definition of the box-counting dimension, equation (8), the quantity $f(\alpha)$ can be interpreted as the fractal dimension of the subset S_α. However, this physical meaning of the function $f(\alpha)$ is not always true (Grassberger, Badii & Politi 1988; Falconer 1990).

It can be shown (Halsey et al. 1996; Martínez et al. 1990) that the quantities q and $\tau(q)$ can be related through a Legendre transformation with α and $f(\alpha)$. These relations are:

$$\alpha(q) = \frac{\mathrm{d}\tau(q)}{\mathrm{d}q}, \tag{13}$$

$$f(\alpha) = q\alpha(q) - \tau(q). \tag{14}$$

To illustrate this section we use the well-known multiplicative multifractal cascade (Meakin 1987; Martínez et al. 1990). The construction of this multifractal is as follows. A square is divided into four equal square pieces and a probability p_i, $(i = 1, \ldots, 4)$, such that $\sum_{i=1}^{4} p_i = 1$, is assigned to each one. Each piece is again subdivided in four small squares, allocating again a value p_i randomly permuted to each one. The measure assigned to each one of the new subsquares is the product of this value of p_i and the corresponding value of its parent square. The subdivision process is continued recursively. In Fig. 1 we show a realization of this

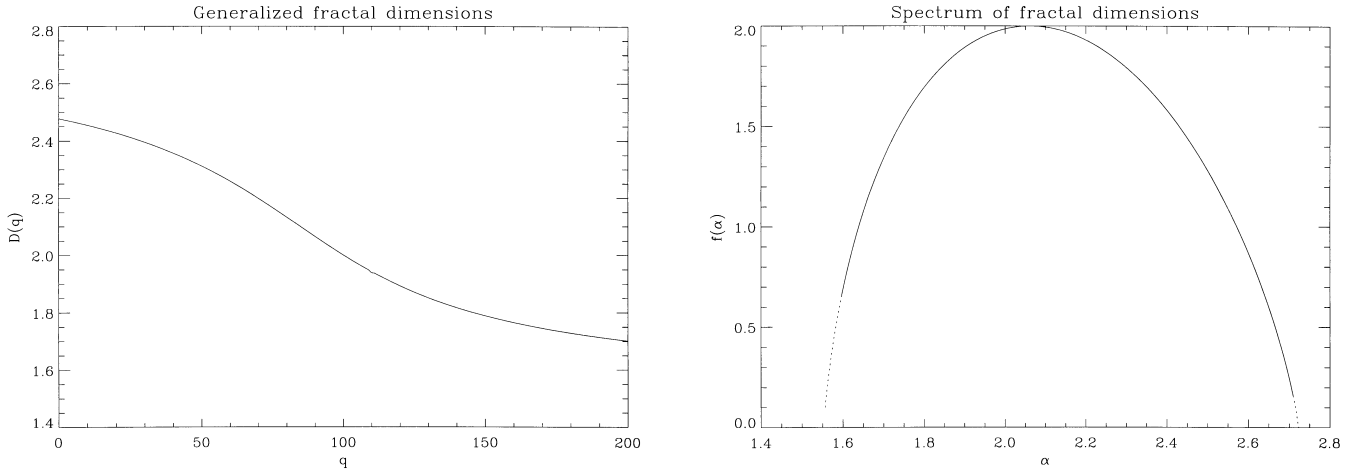

Figure 2. $D(q)$ (left) and $f(\alpha)$ (right) for the multiplicative multifractal. The dotted line on the right panel represents the theoretical $f(\alpha)$ curve for a larger range of q.

multifractal on a grid of 256×256 pixels for the values of the probabilities $p_1 = 0.18$, $p_2 = 0.23$, $p_3 = 0.28$ and $p_4 = 0.31$. We can easily calculate the theoretical values of the multifractal functions $D(q)$ and $f(\alpha)$ for this illustrative example (Martínez et al. 1990). With the multiplicative multifractal we tested the power of the method to recover the true dimensions. In Fig. 2 we show the generalized dimensions $D(q)$ and the corresponding spectrum of fractal dimensions $f(\alpha)$. These curves match perfectly the theoretically expected ones. Note that a single monofractal should render a straight line for $D(q)$ and a single point for $f(\alpha)$.

2.3 Testing Gaussianity

A Gaussian distribution of CMB temperature fluctuations is a generic prediction of inflation. Forthcoming high-resolution maps of the CMB will allow detailed tests of Gaussianity down to small angular scales, providing a crucial test of inflation. Most of the works that analyse CMB maps assume Gaussian initial fluctuations. Kogut et al. (1996) find that the genus, three-point correlation function, and two-point correlation function of temperature maxima and minima are all in good agreement with the hypothesis that the CMB anisotropy on angular scales larger than 7° represents a random-phase Gaussian field. Other alternative methods are proposed, like the angular-Fourier transform (Lewin, Albrecht & Magueijo 1998), Minkowski functionals (Schmalzing & Górsky 1998), correlation of excursion sets (Barreiro et al. 1998), and the bispectrum (Heavens 1998). In an analysis of the 4-year *COBE*–DMR data based on the bispectrum Ferreira et al. (1998) have found that Gaussianity is ruled out at a confidence level in excess of 99 per cent near the multipole of order $l = 16$.

In this section we will test the Gaussianity of the CMB data using an alternative method. The idea is to use the relation between the partition function and the generating function, the last one defined as,

$$G_x(t) = \langle \mathrm{e}^{tx} \rangle. \tag{15}$$

If we know that x is Gaussian distributed then, solving the integral corresponding to the mean value of the previous definition, results:

$$G_x^{\mathrm{Gauss}}(t) = \mathrm{e}^{t\langle x \rangle + \frac{t^2 \sigma_x^2}{2}}. \tag{16}$$

It follows from the last expression that the cumulant function F is

$$F(t) = \ln G(t) = t\langle x \rangle + \frac{t^2 \sigma_x^2}{2}. \tag{17}$$

Finally, the function

$$H(t) = F(t) - t\langle x \rangle - \frac{t^2 \sigma_x^2}{2} \tag{18}$$

should be zero for all t for a Gaussian field.

Let us consider the definition of $Z(q, \delta)$. If the measure is defined as

$$\mu_i^*(\delta) = \mathrm{e}^{\mu_i(\delta)}, \tag{19}$$

with $\mu_i(\delta)$ the same as in Section 2. Then the partition function is

$$Z(q, \delta) = \sum_{i=1}^{N_{\mathrm{boxes}}(\delta)} \mathrm{e}^{q\mu_i(\delta)}, \tag{20}$$

or equivalently,

$$Z(q, \delta) = N_{\mathrm{boxes}}(\delta) \langle \mathrm{e}^{q\mu} \rangle = N_{\mathrm{boxes}}(\delta) G_\mu(q). \tag{21}$$

This relation between $Z(q, \delta)$ and $G_\mu(q)$ allows us to construct the function $H(q)$ which, for a Gaussian measure μ, should be zero for all q at each scale δ. This is a simple way to find non-Gaussian signals. The function $H(q)$ represents the contribution of *all* the moments larger than 2. This contribution should be zero only for a Gaussian field. A plot of this function indicates directly the deviations from Gaussianity.

3 RESULTS: APPLICATION TO *COBE*–DMR DATA

As a practical use of the methods presented we will apply them to the 4-year *COBE*–DMR data.

3.1 Description of the data

We use the *COBE*–DMR 4-year $53 + 90$ GHz maps combination, which is the choice with the largest signal-to-noise ratio (Bennet et al. 1996). These data are in the 'Quad-Cube' pixelization with a pixel size of $\sim 2.^\circ 6$ and the resulting number of pixels is 6144. The data in each pixel represents ΔT in units of mK. The dipole has already been subtracted. Assigned to each pixel there is an

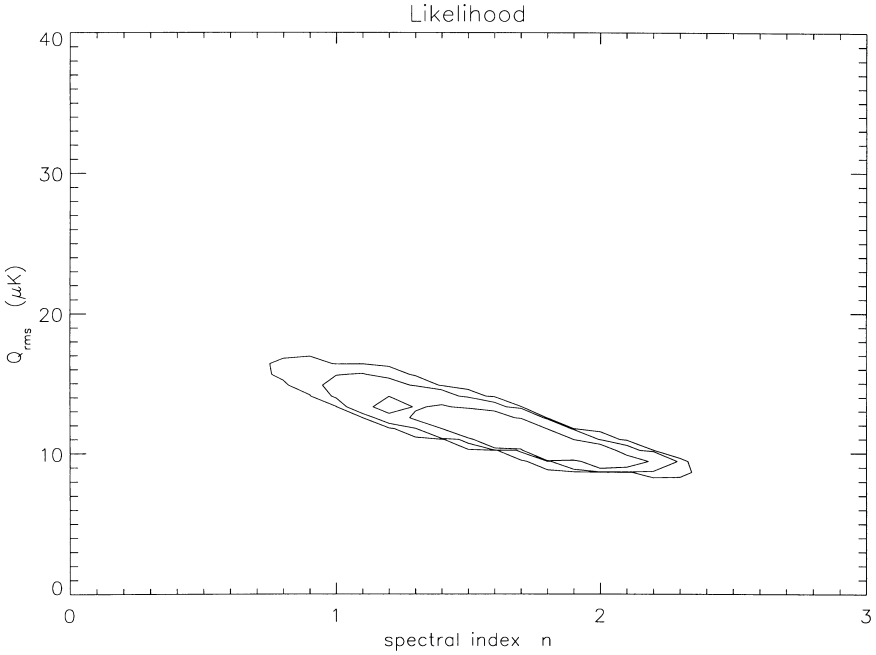

Figure 3. Contour confidence levels (68, 95 and 99 per cent) for the likelihood distribution. The maximum is at $Q_{\rm rms} = 10\,\mu$K and $n = 1.8$.

additional information, the number of times that this part of the sky was explored by the antenna. This information is relevant for the estimation of the instrumental noise.

Part of the data is contaminated by Galactic emission. There is a strip between $\sim \pm 20^\circ$ (in galactic coordinates) in which the Galactic emission dominates the CMB signal. This strip should not be included in the analysis in order to avoid spurious signals. In addition to this strip there are two patches in the sky (one near Orion and the other one in Ophiucus) that show a strong Galactic emission at mm wavelengths (Cayón & Smoot 1995), and should therefore also be removed from the analysis. When this mask is applied, the number of surviving pixels reduces to 3881 from the original 6144.

3.2 Likelihood analysis

In order to determine which are the values of the quadrupole normalization $Q_{\rm rms-PS}$ and the spectral index n that best fit the *COBE* data, we perform Monte Carlo simulations of the CMB maps for a scale-free model with a power spectrum given by $P(k) \propto k^n$, which has variance in the a_{lm} multipoles given by (Bond & Efstathiou 1987):

$$C_l = \frac{4\pi}{5} Q^2_{\rm rms-PS} \frac{\Gamma[l + (n-1)/2]\Gamma[(9-n)/2]}{\Gamma[l + (5-n)/2]\Gamma[(3+n)/2]}. \qquad (22)$$

We consider different values for $Q_{\rm rms-PS}$ and the n ranging from $Q_{\rm rms-PS} = 4\,\mu$K to $Q_{\rm rms-PS} = 35\,\mu$K and from $n = 0.3$ to 2.3. We add instrumental noise based on the number of data collected by *COBE*–DMR at each pixel. Furthermore, there is another effect that must be taken into account, the cosmic variance. To treat conveniently this effect we perform a large number of simulations ($\geq$2000) for each pair of values ($Q_{\rm rms-PS}$, n) and then we compare the average $\mathcal{Z} = \ln Z(q, \delta)$ values of these simulations with the $\mathcal{Z}$ corresponding to the *COBE*–DMR data (the used values for q and δ were $q = -120\,000, -40\,000, 72\,000, 152\,000$ and $\delta = 3, 4, 8, 16$ pixel). The choice for q and δ values is based on the test described in the last part of Section 2.1. The size of the $Z(q, \delta)$ grid, $N_q \times N_\delta$ is not critical and what is now relevant is the q values considered. In particular, high-order moments (i.e. large q) are very sensitive to the tail of the distribution and therefore the results obtained with those high values on the parameter estimates are not stable. The combination of q and δ values, was one of the combinations for which the recovered parameters $Q_{\rm rms}$ and n were closer to the input parameters and with smaller error bars. As mentioned in Section 2, q should take values of order 10^5 in order to distinguish between models with temperature fluctuations of order 10^{-5}. The values of q where chosen to be asymmetric in an attempt to consider possible asymmetries that could exist between the negative and positive temperature fluctuations. The range for δ runs from 2 pixels (approximately the antenna size) to 24 pixels which is the largest box size required to have at least 8 boxes. Using a maximum likelihood method one can determine which are the best-fitting parameter values of the simulations (signal + noise) to the *COBE*–DMR data.

In Fig. 3 we show a contour plot of the likelihood obtained for the *COBE*–DMR data. The maximum is at $Q_{\rm rms-PS} = 10^{+3}_{-2.5}\,\mu$K and $n = 1.8^{+0.35}_{-0.65}$ (95 per cent marginalized errors) and the contour level at 68 per cent is compatible with the assumed standard value $Q_{\rm rms-PS} = 18 \pm 3\,\mu$K for the Einstein–de Sitter model with a scale invariant primordial spectrum of density perturbations, $n = 1$. The various analysis of the 4-year *COBE* data when combined give as the best-fitting parameters $Q_{\rm rms-PS} = 15.3^{+3.8}_{-2.8}\,\mu$K and $n = 1.2 \pm 0.3$. The result presented here predicts larger values of n and smaller values of $Q_{\rm rms-PS}$ than the result indicated above (although always inside the anticorrelation law for the two parameters). This result is in agreement with the one found by Smoot et al. (1994), using a similar approach. Smoot et al. (1994) found for the best fit, $Q_{\rm rms-PS} = 13.2 \pm 2.5\,\mu$K and $n = 1.7^{+0.3}_{-0.6}$. A possible explanation for the discrepancy between our results and those obtained with the standard methods could be a bias present in the likelihood estimator. In the tests of our algorithm we found a systematic bias in the marginalized likelihood functions both for $Q_{\rm rms}$ and n with typical values of $\delta n \sim +0.2$ and

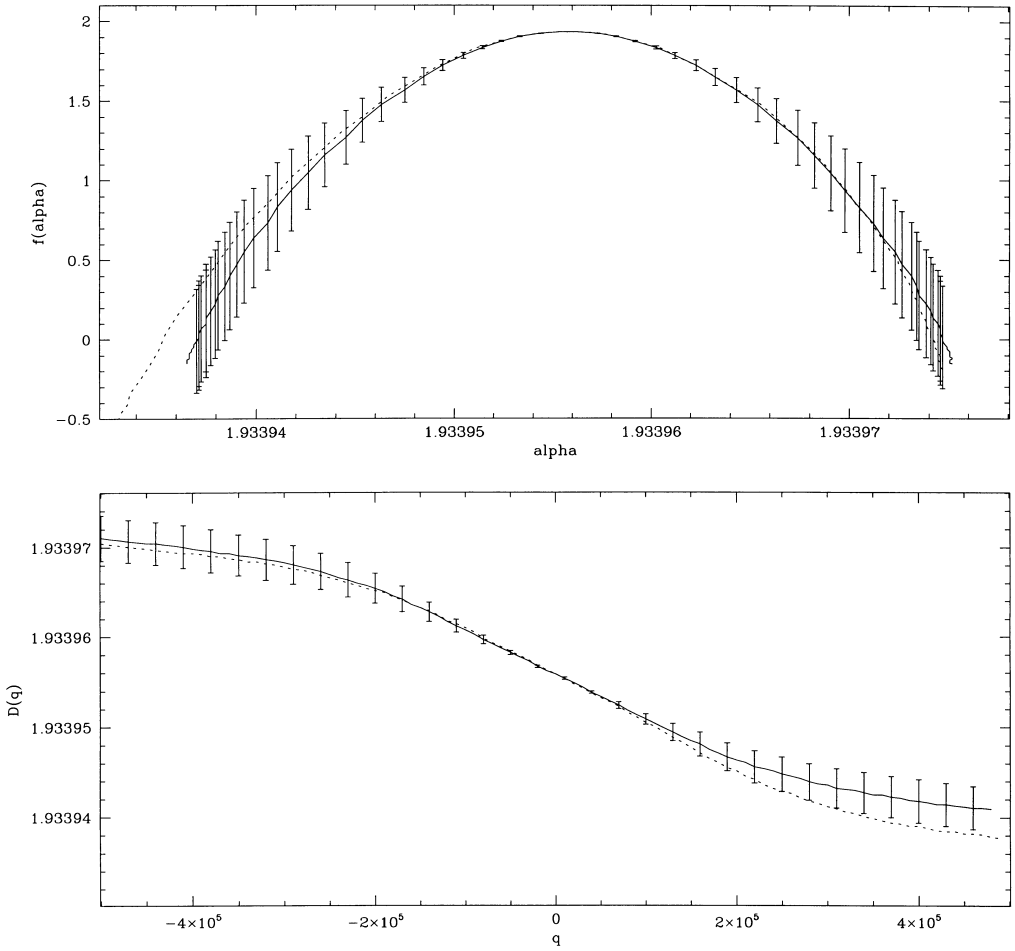

Figure 4. $D(q)$ (bottom) and $f(\alpha)$ (top) curves for *COBE*–DMR (dotted line) and for one model with $Q_{\rm rms} = 15\,\mu$K and $n = 1.2$.

$\delta Q_{\rm rms} \sim -2$ which could explain part of our discrepancy. The reason for this bias can be the difference between the assumed Gaussian form for the likelihood of the partition function in equation (4) and the real non-Gaussian distribution. The probability distribution of the $\mathcal{Z}$ at each (q, δ) obtained from simulations is similar to a Gaussian probability distribution but with a longer tail for high values. We also think that maybe the noise can contribute to that bias. The high-order moments (large q) of the partition function are very sensitive to the tails of the distribution of the temperature fluctuations. A low signal-to-noise ratio (as is the case for the *COBE*–DMR data) could raise the parameter n that best fit the *COBE*–DMR data. We did some tests in this direction and apparently the noise can increase the value of n (and consequently can produce a lower value of $Q_{\rm rms}$).

3.3 Multifractal analysis

We apply the formalism of Section 2.2 to the simulations and to the *COBE*–DMR data. In Fig. 4 we plot $D(q)$ and $f(\alpha)$ for the *COBE*–DMR and for one model ($Q_{\rm rms-PS} = 15\,\mu$K, $n = 1.2$) inside the $Q_{\rm rms-PS}$–n degeneration with its error bars. The $D(q)$ curve has been obtained by fitting a power law to the partition function in the range of scales $2 \leq \delta \leq 24$ pixels, following equations (9) and (10) . Note that the value of $D(0)$ is not 2 as it would be expected for a continuous bidimensional surface. The mask slightly lowers this value.

By means of a Legendre transform (equations 13 and 14) we have obtained the corresponding $f(\alpha)$ curve. A narrow $f(\alpha)$ curve means a very homogeneous data. If the measure associated to the data is multifractal in nature, these curves should be the same for all the scale ranges. We have found that this is not the case for the *COBE*–DMR data. The multifractal curves corresponding to different scale ranges do not match each other. CMB simulations without noise show the same behaviour. The reason for that lies in the fact that a scaling like that in equation (9) is not present. This can be illustrated by looking at the behaviour of the local slopes of $\ln Z(q, \delta)$ versus $\ln \delta$. In Fig. 5 we show the change in the *reduced* slopes $(\tau(q, \delta)/(q - 1))$ as a function of the scale for a fixed value of the parameter q for the *COBE*–DMR data. For this plot the analysis was performed only in the top and bottom faces of the Quad-Cube which are not affected by the mask. For a multifractal measure these curves should be horizontal straight lines. As we can appreciate in the left panel, this is not the case for the *COBE*–DMR data. The result for a simulation without noise is shown in the right panel. In both cases, we do not see a neat plateau for large absolute values of q. However it is not clear whether the fluctuations of the local reduced slopes are just due to numerical noise related to the resolution of the maps (i.e. the limited number of pixels) or, on the contrary, these fluctuations are intrinsic to the measure and, therefore, prove that the measure is not a multifractal. Although our result neither support nor contradict this interpretation, it seems more natural to expect fractal behaviour in the case that one is using

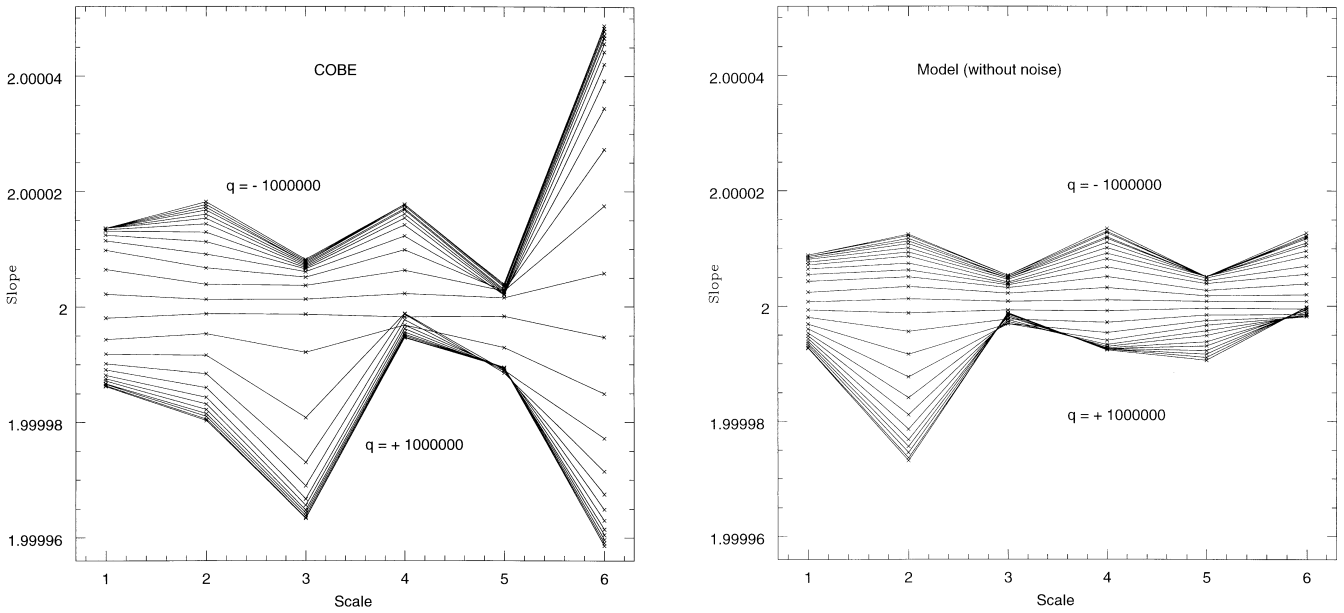

Figure 5. *Reduced* slopes computed between two consecutive scales for the *COBE*–DMR data (left) and for simulated data (without noise, right). Each curve corresponds to a fixed value of q betwen -10^6 and 10^6.

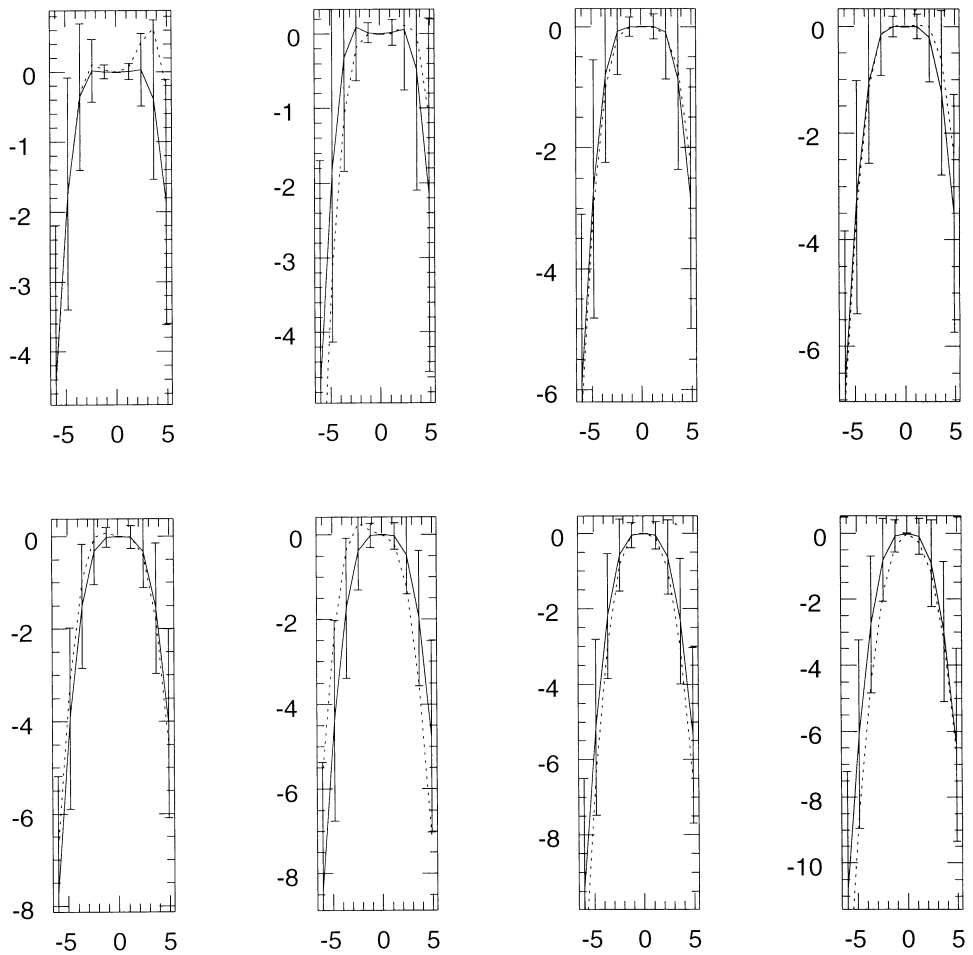

Figure 6. $H(q)$ curves for eight different scales. From left to right and from top to bottom. 2×2 pixels to 24×24 pixels. The x-axis represents the values of q.

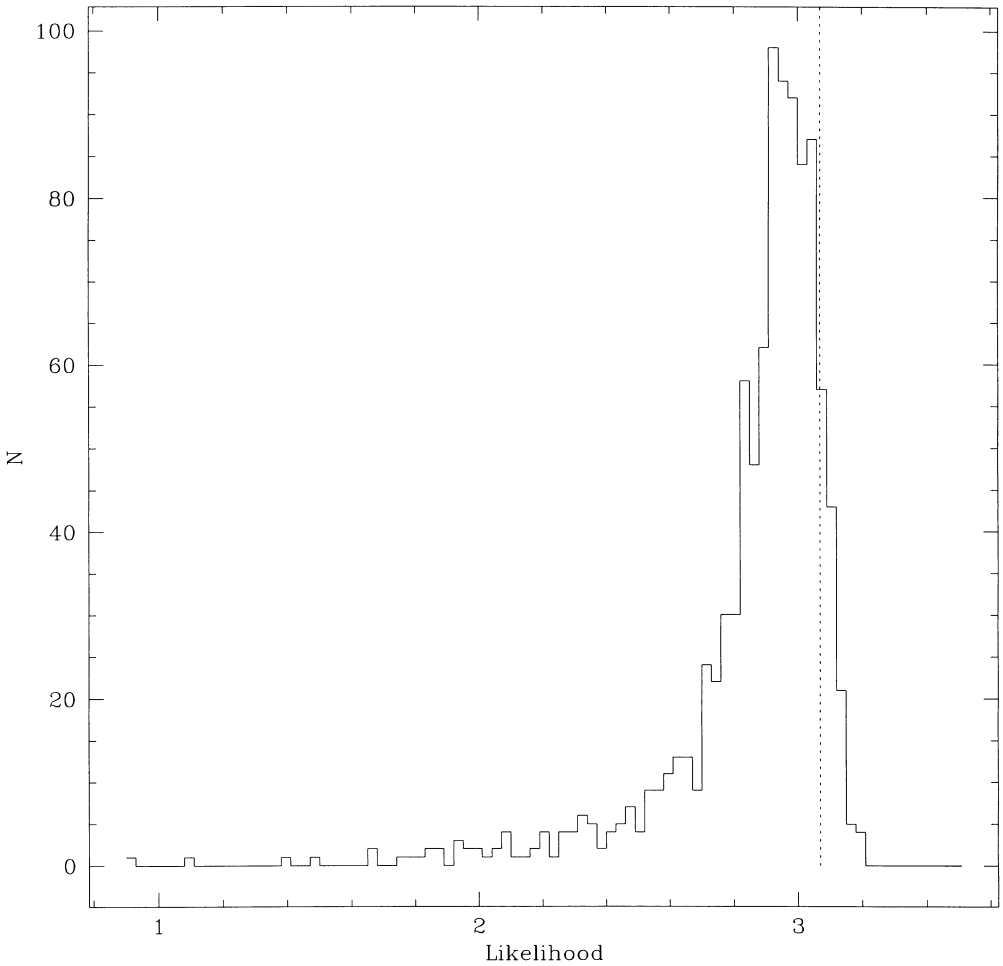

Figure 7. Likelihood distribution for 1000 simulations for the best-fitting model in Section 3.2. The value corresponding to the *COBE*–DMR data is shown as a dotted line and is in clear agreement with the Gaussian hypothesis.

the absolute value of the relative temperature fluctuations $\Delta T/T$ as the measure (Mollerach et al. 1998). As shown in that paper, $\Delta T/T$ fluctuations generated by the Sachs–Wolfe effect behave like a fractional brownian fractal.

3.4 Gaussianity

To test whether the *COBE*–DMR data are Gaussian distributed, we compare the $H(q)$ curve for *COBE*–DMR with those curves arising from the best-fitting CMB Gaussian models obtained in Section 3.2. In Fig. 6 we show the plots of $H(q)$ for different grid scales. For each realization, the measure is rescaled in order to have dispersion equal to one. This allows to have a small and equal range of q values for all scales. We would like to point out the deviation of the mean value from zero when q moves away from zero. This is due to the fact that we have a finite number of pixels (i.e. a cosmic variance effect). The predicted behaviour of equation (15) is only true when we compute the mean over infinite values (or equivalently, solve the integral between $-\infty$ and $+\infty$). Otherwise $H(q)$ is not zero at large values (positive and negative) of q. Fig. 7 shows the likelihood distribution of the 1000 Gaussian realizations (with noise) and the dotted line corresponds to the *COBE* value. It is clear that the *COBE*–DMR is perfectly compatible with the Gaussian hypothesis.

4 DISCUSSION AND CONCLUSIONS

We have shown in this work the power of the partition function to describe CMB maps taking into account the information given at different scales and by different moments. We have also shown the flexibility of such a function to be used in various analyses: standard likelihood, multifractal and Gaussian. We applied these analyses to the 4-year *COBE*–DMR data.

Based on the likelihood function we find the best-fitting parameters $Q_{\rm rms-PS} = 10^{+3}_{-2.5}\,\mu$K and $n = 1.8^{+0.35}_{-0.65}$. It is remarkable the agreement between our work and the one by Smoot et al. (1994).

The *COBE*–DMR data (and the simulations of scale-invariant power spectrum) do not show a fractal behaviour, regarding the absolute temperature map. On the other hand, recent galaxy surveys covering large scales (> 100 Mpc) do not show either a fractal behaviour (Wu et al. 1998). Both results allow to conclude that neither the mass distribution (assuming a linear bias) nor the intensity of the CMB show a fractal behaviour on large scales. The partition function analysis performed shows no evidence for non-Gaussianity in the *COBE*–DMR data. This is in agreement with all the previous analyses of the *COBE*–DMR data except the one by Ferreira et al. (1998). Simulations done at higher resolution have shown the power of this method to discriminate between

Gaussian and non-Gaussian signals. That analysis will be presented in a future paper.

Finally, we would like to remark that the likelihood analysis based on the partition function is computationally intensive. Actually a non-optimized code applied to the *COBE*–DMR data takes a few days (CPU time) to run in an Alpha server 2100 5/250. Moreover, the computation of the partition function increases with the number of pixels N as $O(N)$. This rate should be compared with the most widely applied method used to compress data and to estimate cosmological parameters, the power spectrum of the fluctuations. The direct computation of the power spectrum goes like $O(N \log N)$ (this behaviour is a result of the FFT). Standard brute-force approaches used to estimate the power spectrum go like $O(N^3)$. The reason for this $O(N^3)$ rate is the matrix inversion and determinant calculation whose dimension grows as the number of pixels. On the contrary, in the partition function likelihood analysis the number of bins (or matrix dimension) of the likelihood is $N_q \times N_\delta$, being this number usually well below one thousand (even for high-resolution maps). The number of moments q is an arbitrary parameter independent of N and the number of scales δ increases as $\leq O(N^{1/2})$. The process of inverting the correlation matrix is clearly reduced in the case of the partition function. This point makes the method useful for forthcoming large data-sets. One can therefore consider the partition function as an alternative way to compress large data sets. Furthermore, for the general situation of non-Gaussian data sets, the partition function is clearly preferable to the power spectrum since the former contains information on several moments of the data.

ACKNOWLEDGMENTS

We would like to thank R. B. Barreiro for kindly providing her program for the simulations, L. Cayón for help dealing with the *COBE*–DMR maps and interesting discussions. SM acknowledges CONICET for financial support and to the Vicerrectorado de Investigacion de la Universidad de Valencia. JMD thanks the DGES for a fellowship. This work has been financially supported by the Spanish DGES, project n. PB95-1132-C02-02 and project n. PB96-0797, and by the Spanish CICYT, project n. ESP96-2798-E. The *COBE* data sets were developed by the NASA Goddard Space Flight Center under the guidance of the *COBE* Science Working Group and were provided by the NSSDC.

REFERENCES

Barreiro R. B., Sanz J. L., Martínez-González E., Cayón L., Silk J., 1997, ApJ, 478, 1
Barreiro R. B., Sanz J. L., Martínez-González E., Silk J., 1998, MNRAS, 296, 693
Bennet C. L. et al., 1996, ApJ, 464, L1
Bond J. R., Efstathiou G., 1987, MNRAS, 226, 655
Bond J. R., Efstathiou G., Tegmark M., 1997, MNRAS, 291, L33
Borgani S., 1995, Phys. Rep., 251, 1
Cayón L., Smoot G. F., 1995, ApJ, 452, 487
Cayón L., Martínez-González E., Sanz J. L., Sugiyama N., Torres S., 1996, MNRAS, 279, 1095
Davis M., 1997, in Turok N., ed., Critical Dialogues in Cosmology. World Scientifc, Singapore, p. 13
De Gouveia dal Pino E. M., Hetem A., Horvath J. E., De Souza C. A. W, Villela T., De Araujo J. C. N., 1995, ApJ, 442, L45
Durrer R., Kunz M., Lineweaver C., Sakellariadou M., 1997, Phys. Rev. Lett., 79, 5198
Fabbri R., Torres S., 1996, A&A, 307, 703
Falconer K. J., 1990, Fractal Geometry, Mathematical Foundations and Applications. John Wiley & Sons, Chichester
Feder J., 1988, Fractals. Plenum Press, New York, p. 233
Ferreira P. G., Magueijo J., Górski K. M., 1998, ApJ, 503, L1
Frisch U., Parisi G., 1985, in Ghil M.,Benzi R., Parisi G., eds, Turbulence and Predictability in Geophysical Fluid Dynamics and Climate Dynamics. North-Holland, New York
Grassberger P., Badii R., Politi A., 1988, J. Stat. Phys., 51, 135
Gutiérrez de la Cruz C. M., Martínez-González E., Cayón L., Rebolo R., Sanz J. L., 1994, MNRAS, 271, 553
Guzzo L., 1997, New Astron., 2, 517
Halsey T. C., Jensen M. H., Kadanoff L. P., Procaccia I., Shraiman B. I., 1986, Phys. Rev. A, 33, 1141
Heavens A. F., 1998, MNRAS, submitted (astro-ph/9804222)
Hinshaw. G., Banday A. J., Bennet C. L., Górski K. M., Kogut A., Smoot G. F., Wright E. L., 1996a, ApJ, 464, L17
Hinshaw G., Banday A. J., Bennet C. L., Górski K. M., Kogut A., Lineweaver C. H., Smoot G. F., Wright E. L., 1996b, ApJ, 464, L25
Hobson M. P., Jones A. W., Lasenby A. N., 1998, MNRAS, submitted (astro-ph/9810200)
Jensen M. H., Kadanoff L. P., Libchaber A., Procaccia I., Stavans J., 1985, Phys. Rev. Lett., 55, 2798
Jones B. J. T., Martínez V. J., Saar E., Einasto J., 1988, ApJ, 332, L1
Kogut A., Banday A. J., Bennet C. L., Górski K. M.,Hinshaw G., Smoot G. F., Wright E. L., 1996, ApJ, 464, L29
Lewin A., Albrecht A., Magueijo J., 1998, preprint (astro-ph/9804283)
Mandelbrot B. B., 1974, J. Fluid. Mech., 62, 331
Martínez V.J., Jones B.J.T., Domínguez-Tenreiro R., van de Weygaert R., 1990, ApJ, 357, 50
Martínez V. J., Pons-Bordería M. J., Moyeed R. A., Graham M. J., 1998, MNRAS, 298, 1212
Meakin P., 1987, Phys. Rev. A, 36, 2833
Mollerach S., Martínez V. J., Diego J. M., Martínez-González E., Sanz J. L., Paredes S., 1998, ApJS, submitted
Pando J., Valls-Gabaud D., Fang L., 1998, Phys. Rev. Lett., 81, 4568
Pietronero L., Montuori M., Sylos-Labini F., 1997, in Turok N., ed., Critical Dialogues in Cosmology. World Scientific, Singapore
Pompilio M. P., Bouchet F. R., Murante G., Provenzale A., 1995, ApJ, 449, 1
Scaramella R. et al., 1998, A&A, 334, 404
Schmalzing J., Górsky K. M., 1998, MNRAS, 297, 355
Schuster H. G., 1989, Deterministic Chaos. VCH, Weinheim
Smoot G. F., Tenorio L., Banday A. J., Kogut A., Wright E. L., Hinshaw G., Bennet C. L., 1994, ApJ, 437, 1
Sreenivasan K. R., Menevau C., 1988, Phys. Rev. A, 38, 12, 6287
Tegmark M., 1996, ApJ, 464 L35
Torres S., Cayón L., Martínez-González E., Sanz J. L., 1995, MNRAS, 274, 853
Vicsek T., 1989, Fractal Growth Phenomena. World Scientific, Singapore
Winitzki S., Kosowsky A., 1997, New Astron., submitted (astro-ph/9710164)
Wright E. L., Bennet C. L., Górski K. M., Hinsaw G., Smoot G. F., 1996, ApJ, 464, L21
Wu K.K.S., Lahav O., Rees M.J., 1999, Nat, 397, 225

This paper has been typeset from a TEX/LATEX file prepared by the author.